Materials Research Proceedings 54 (2025) 799-808 https://doi.org/10.21741/9781644903599-86

Modeling of charge welds evolution through Cahn-Hilliard equation for interaction between different Fluids: Experimental-numerical comparison with industrial case studies

Sara Di Donato[1,a*], Riccardo Pelaccia[2,b], Marco Negozio[3,c], Barbara Reggiani[2,4,d] and Lorenzo Donati[1,e]

[1]University of Bologna - DIN Department of Industrial Engineering, Viale Risorgimento 2, 40136, Bologna, Italy

[2]University of Modena and Reggio Emilia - DISMI Department of Sciences and Methods for Engineering, Via Amendola 2, 42122, Reggio Emilia, Italy

[3]University of Parma - DISTI Department for Industrial Systems and Technologies, Parco Area delle Scienze, 181/A, 43124 Parma, Italy

[4]University of Modena and Reggio Emilia - InterMech - MO.RE, Piazzale Europa 1, Reggio Emilia 42124, Italy

[a]sara.didonato2@unibo.it, [b]riccardo.pelaccia@unimore.it, [c]marco.negozio@unipr.it, [d]barbara.reggiani@unimore.it, [e]l.donati@unibo.it

Keywords: Extrusion, Charge Welds Defects, Advanced Numerical Simulation, Aluminum Alloys

Abstract. In the hot extrusion process for metals, the interaction between the old and new billet materials during each cycle contaminates a specific length of the extruded profile. Experimental analysis of defect evolution is both time-intensive and costly, while empirical industrial methods and analytical formulas lack the precision required in scenarios where minimizing scrap is critical. To address this, a numerical model was developed using COMSOL Multiphysics® software, coupling the Navier-Stokes equations with the Cahn-Hilliard equation to investigate the interaction between two immiscible fluids with very high viscosities—representing the old and new billet materials. The model's accuracy was validated through four industrial case studies, that varied in terms of profile-shape complexity and material extruded.

Introduction

During the direct extrusion, billets are continuously loaded into a press and joined under high hydrostatic pressure, forming a single extruded profile. This process leads to the formation of a transition zone between successive billets, where the material from the preceding billet interacts with the material of the new billet. The formation of this zone is a critical aspect of the extrusion process and is commonly referred to as the charge weld defect, transverse weld, or front-end defect. Given the nature of the process, it is not possible to avoid the charge zone, which typically begins after the stop mark (the permanent marker on the profile indicating the end of a billet stroke) and extends along the profile to a variable length, depending on the die design and processing parameters [1]. The charge transition zone typically exhibits contamination due to residues such as oxides, dust, or lubricants accumulated during billet loading. As a result, the material in this region must be discarded, as it fails to meet the required mechanical properties for industrial applications. Reducing material waste due to charge welds is paramount for improving the efficiency and sustainability of aluminum profile production [2,3]. Despite advancements in manufacturing processes, the defects associated with charge welds continue to challenge process optimization and economic viability. In the past, the evaluation of charge weld zones relied on the experience and intuition of extrusion operators or labor-intensive trial-and-error experiments.

However, recent advancements have introduced numerical methods to predict and mitigate charge weld formation, improving process reliability and reducing waste. Several numerical investigations have been conducted to study charge welds in solid and hollow profiles. Early efforts included 2D simulations employing the Lagrangian method to analyze the relationship between extrusion parameters and charge weld formation[4,5]. More advanced studies utilized Finite Element (FE) models and 3D Arbitrary Lagrangian–Eulerian (ALE) simulations to explore the defect evolution under various die designs and process parameters [6–11]. However, the behavior and mechanisms of charge weld formation have not yet been fully understood, limiting the effectiveness of current control strategies from both economic and sustainable manufacturing perspectives. In the context of Finite Element Method (FEM) simulations, COMSOL Multiphysics has emerged as a versatile tool in academic and industrial research for modeling complex manufacturing processes. Unlike dedicated commercial software tailored for specific manufacturing scenarios, COMSOL offers the flexibility to implement customized models, enabling the analysis of diverse aspects of the extrusion process, such as the interaction between different fluids to replicate the effect of lubricants. In a previous study, Di Donato et al. [12] developed an innovative predictive model for billet-to-billet interaction within the COMSOL Multiphysics environment. This model employed the Phase Field Method to simulate the interface behavior of two immiscible fluids at high viscosity, dependent on temperature and strain rate.

The present study extends the previous work by demonstrating the flexibility and accuracy of the predictive model through four distinct industrial case studies: extrusion of two hollow profiles using AA6060 and AA6082 alloys, and two solid profiles made by AA6063 and AA6082. The study focuses on validating the model's predictions for charge weld formation under diverse geometric and process conditions. By emphasizing the predictive model’s adaptability and accuracy, this research aims to provide a comprehensive framework for optimizing the extrusion process, thereby contributing to the development of more sustainable and efficient manufacturing practices.

Experimental Procedures

For each case study, industrial extrusion campaigns were conducted to produce the profiles under controlled manufacturing conditions. The relevant extrusion process parameters are summarized in Table 1 for all case studies. Subsequently, detailed analyses of the extruded charge weld defects were performed in the laboratory to evaluate its evolution.

Extrusion Case study A [13,14] investigated the extrusion of an AA6060 hollow profile produced by Profilati Spa (Emilia Romagna, Italy). The cross-sectional geometry of this profile is illustrated in Fig. 1*A*.

Extrusion Case study B [15,16] focused on the extrusion of three tube-shaped profiles made from AA6082 alloy, as shown in Fig. 1*B*. The die utilized for these profiles was fabricated by Almax Mori (Rovereto, Italy), while the extrusion was performed by the Metra company in Rodengo Saiano, Italy.

Extrusion Case Study C [10,17] involves the extrusion of a solid profile made from AA6063 alloy, conducted by Indinvest LT S.r.l. (Latina, Italy). The profile featured a central thick section with a thin jagged appendage and a small bulge located at opposite ends of the top side, as shown in Fig. 1*C*. Two identical profiles were extruded simultaneously using a flat two-hole die.

Extrusion Case Study D [11] examines the extrusion of a solid AA6082 profile characterized by a thick section with a large side wing, as shown in Fig. 1*D*. The experimental campaign was also carried out at the Indinvest LT S.r.l. plant (Latina, Italy).

Therefore, the analyzed profiles exhibited differences in geometry and material composition: two industrial hollow profiles, one with a more complex geometry made from AA6060 alloy and another simpler geometry extruded using a three-opening die with AA6082 alloy, and two solid profiles made from AA6063 and AA6082 alloys, respectively.

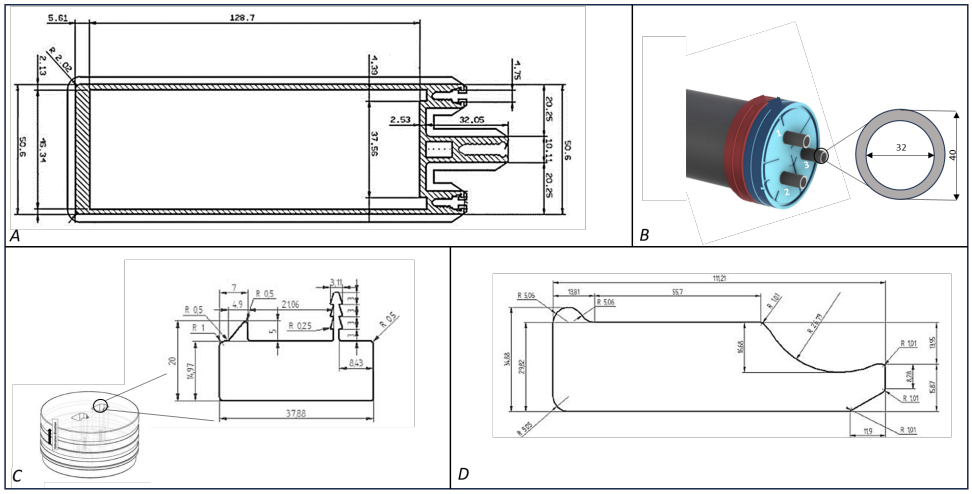

Figure 1 – Extrusion Case Studies geometries (all quotes are in [mm]).

Table 1 – Extrusion process parameters of case studies A, B, C and D.

Process parameters	Extrusion case study A	Extrusion case study B	Extrusion case study C	Extrusion case study D
Profile alloy	AA6060	AA6082	AA6063	AA6082
Extrusion ratio	27	45	44	20
Ram speed [mm/s]	8/12	4.4	6.44	7.64
Billet temperature [°C]	480	440	480	480
Die temperature [°C]	510	480	450	450
Container temperature [°C]	430	390-425	430	440
Billet length [mm]	950	680	670	990
Billet diameter [mm]	203	279	254	254
Container diameter [mm]	211	286	264	264
Billet rest length [mm]	44	30	15	15

Fig. 2 illustrates a scheme of the defect evolution within the profile section where material from the old billet is replaced by that of the new billet. The red line delineates the transition zone between the two materials, representing the welding line identified through etching during the experimental analysis. The stop mark serves as a reference point: negative values correspond to distances along the extrusion direction, while positive values indicate distances toward the press. The charge weld defect originates near the stop mark, specifically in the region with positive distances where material from the new billet begins to flow into the extruded profile. The extent of the charge weld defect was evaluated based on the assumption that its disappearance occurred when 95% of the old billet material had been replaced with the new billet, aligned with industrial practices. During the experimental campaign, several billets were extruded for each case study, and the evolution of the defects was evaluated when the standard operating conditions were reached (steady-state conditions in terms of thermal field and extrusion load). In this study, the transition between billets 3 and 4 was considered for case studies A [13,14] and B [15,16], and the transition between billets 6 and 7 for case studies C [10,17] and D [11]. To investigate the behavior of charge weld defects, each extruded profile was initially sectioned into 100 mm length specimens. Moreover, for Case Studies C and D, where rapid defect propagation was expected due to solid geometry, the 100 mm specimens were further subdivided for a more detailed investigation. Each specimen was polished using abrasive papers and then etched in a sodium hydroxide solution (300 g NaOH per liter of H_2O, heated to 60 °C, with etching durations of about 90 seconds) to expose the presence of new billet material in the cross-section. Digital images of each section were captured, the defect-containing areas were identified, and the proportion of new billet material in each cross-section was measured using image analysis software.

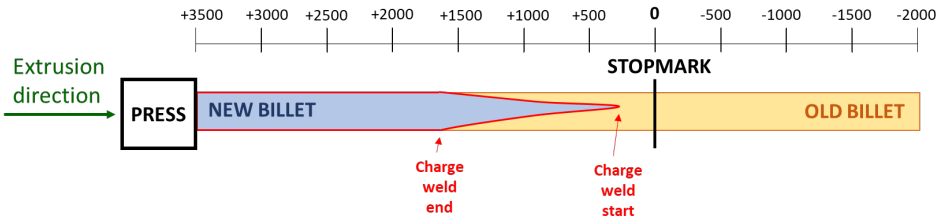

Figure 2 – Diagram of the interaction between the old and new billet material.

Numerical Modeling

The numerical model was developed using COMSOL Multiphysics with a pure Eulerian approach, keeping the mesh fixed during calculations [12]. The laminar flow module, to treat the aluminum as Non-Newtonian fluid at very high viscosity depended on strain rate and temperature, and the Heat Transfer with Solid and Fluid module, to consider the heat generated by friction forces and the deformation energy, are coupled to simulate the extrusion process. Main simulation parameters are summarized in Table 2. The container, that encompasses the billet, and the ram, that forces the billet to be deformed within the die, are replaced with equivalent thermal and frictional boundary conditions in order to reduce computational time. Thermal interactions were modeled by replacing conduction between the material and tooling with equivalent convection using a heat transfer coefficient of 11000 W/(m²·K), typical for aluminum-steel interfaces [18,19]. While a convective heat exchange of 100 W/(m²·K) with air at 150 °C was applied in areas where the material was not in contact with the die [20]. For friction, a sticking condition was applied in the contact zone between the deformed material and tooling set, except for the bearing surfaces, where a slip condition was defined with a friction factor dependent on aluminum viscosity [20,21].

Table 2 – Extrusion simulation parameters.

Simulation Parameters	Extrusion case study A	Extrusion case study B	Extrusion case study C	Extrusion case study D
Billet Temperature [°C]	480	440	480	480
Die Temperature [°C]	510	480	450	450
Container Temperature [°C]	430	420	430	440
Ram Temperature [°C]	440	430	380	380
Air temperature at the profile exit [°C]	150	150	150	150
ϕ	-1 new billet material/+1 old billet material			
σ_{st} [mN/m]	1e7	1e7	1e7	1e7
χ [m·s/kg]	1e-8	1e-8	1e-8	1e-8
ε [m]	0.0005	0.0005	0.0005	0.0005

To simulate charge weld evolution, the Navier-Stokes equations, which predict the velocity field of material flow under deformation, were coupled with the Cahn–Hilliard equation [22,23], to fully describe the interaction between two immiscible fluids (new and old billet material). Therefore, the material flow under deformation was divided into two regions, distinguishing between the new and old billet material The dimensionless phase field parameter ϕ, governed by the partial differential equation as expressed in Eq. 1, ranged from -1 to 1, representing respectively the first and second fluids.

$$\frac{\delta\phi}{\delta t} + u \cdot \nabla\phi = \nabla \cdot \gamma\nabla G, \quad (1)$$

where u is the advective velocity fields calculated via the Navier–Stokes equations.

The mobility γ [m³·s/kg] is calculated as in Eq. 2 and depends on the mobility tuning parameter χ [m·s/kg], and on the interface thickness δ_i [m].

$$\gamma = \chi{\delta_i}^2. \quad (2)$$

The chemical potential G [Pa] is expressed as in Eq. 3 where λ [N] is the mixing density energy.

$$G = \lambda\left[-\nabla^2\phi + \frac{\phi(\phi^2-1)}{{\delta_i}^2}\right];\ \lambda = \frac{3\sigma_{st}\delta_i}{2\sqrt{2}}. \quad (3)$$

Although the model incorporated the dependence of density and viscosity on ϕ, this was negligible since the new and old billet materials have identical properties.

For accurate prediction of charge weld evolution, the calibration of the interface thickness ε and the interaction between the two fluids, governed by the mobility tuning parameter χ and surface tension σ_{st} is critical. Increasing ε reduces computational time but compromises the accuracy of the interface shape. Conversely, selecting an ε value smaller than the mesh element size may lead to numerical instability. In this study, ε was set to 0.5 mm, corresponding to half the average mesh element size of the initial interface. The other parameters were calibrated to effectively model the interaction between deforming solids during extrusion, even if they have been numerically modeled as fluid at high viscosity. A sufficiently low value of χ (1e-8 m·s/kg) was chosen to prevent the formation and diffusion of discrete particles. At the same time, a sufficiently high value of σ_{st} (1e7 mN/m) was assigned.

Results and Discussion

Fig. 3, Fig. 4, Fig. 5, and Fig. 6 present the experimental analyses conducted on the extruded profiles, highlighting the material of the new billet in red. The accuracy of the numerical model implemented within COMSOL environment was demonstrated in a previous work by Di Donato et al. [12], where an experimental-numerical comparison in terms of extrusion load, profile temperature, and velocity field was conducted for the *Extrusion Case studies A and B*. In this work, the accuracy of the model is examined exclusively in predicting the charge weld defect in relation to the four experimental extrusion cases. The graphs in Fig. 7 and Fig. 8 present the numerical-experimental comparison for predicting the charge weld defect in the four examined case studies. The defect evolution is indicated as the percentage of new billet material plotted against the distance from the stop mark, with experimental data shown by a solid line with markers and numerical results represented by a dashed line.

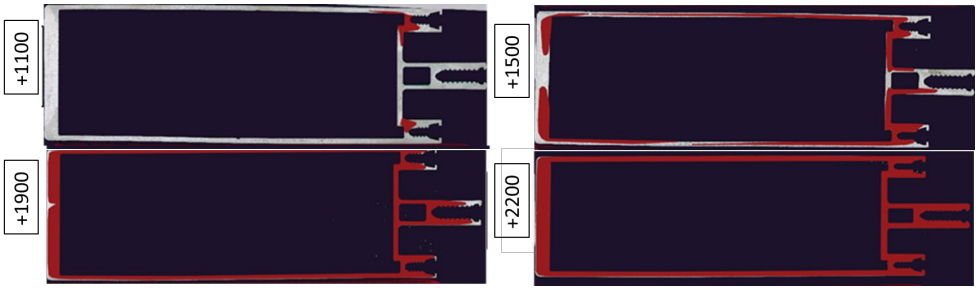

Figure 3 – Charge weld evolution Extrusion Case study A. Distances from the stop mark in [mm]. The experimental data obtained from [24].

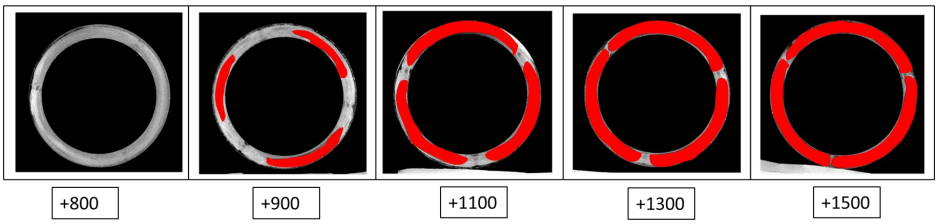

Figure 4 – Charge weld evolution Extrusion Case study B. Die exit 3. Distances from the stop mark in [mm]. The experimental data obtained from [16].

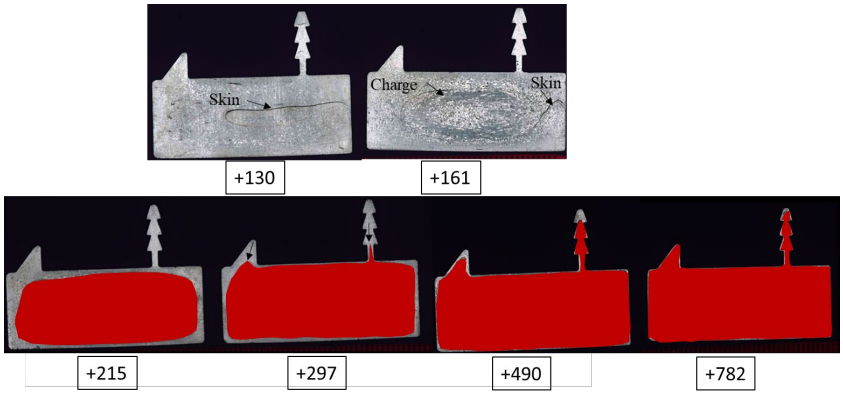

Figure 5 – Charge weld evolution Extrusion Case study C. Distances from the stop mark in [mm]. The experimental data obtained from [10].

Figure 6 – Charge weld evolution Extrusion Case study D. Distances from the stop mark in [mm]. The experimental data obtained from [11].

Regarding the *Extrusion Case Study A*, analysis of the graph, represented in blue, reveals that the simulation closely captures the defect progression, predicting its onset at 900 mm, compared to the experimentally observed 975 mm (resulting in a prediction error of 7.6%). For the extent, the simulation forecasted the defect to reach 2700 mm, whereas the experimental observation extended to 2500 mm (resulting in a prediction error of 7.4%). Fig. 9A also presents the numerical trends in the evolution of charge welds, providing a visual representation of the charge weld morphology to validate the Phase Field model predictions. The comparison indicates a significant correspondence in the initiation and spread of the defect across the cross-section of the profile. Specifically, the simulation accurately anticipates the defect onset within the inner region of the side wings, its expansion to contaminate the no-wings side at 1500 mm, and subsequent contamination of the entire profile area.

Similar results were observed in *Extrusion Case Study B*, represented by the green graph in Fig. 7. The graph compares the numerical and experimental trends of charge welds for Profile 3, revealing that the prediction reliably describes the defect evolution. The experimental observation indicated the onset of the new billet material at 800 mm and its extent to 2050 mm, while the simulation predicted an onset at 775 mm and an extent to 2000 mm (with prediction errors of 3.1% for onset and 2.4% for extent). Visually, Fig. 9B shows the numerical prediction of a defect evolution originating between the seam welds, generating three initiation points approximately 900 mm, from which the defect extends until complete billet material replacement. Notably, the numerical predictions for both case studies slightly underestimate the defect onset and extent. This discrepancy may arise from the high challenge of experimentally detecting defect evolution in thin-thickness, complex profiles, potentially leading to an underestimation of the actual values, especially when material replacement is nearly complete.

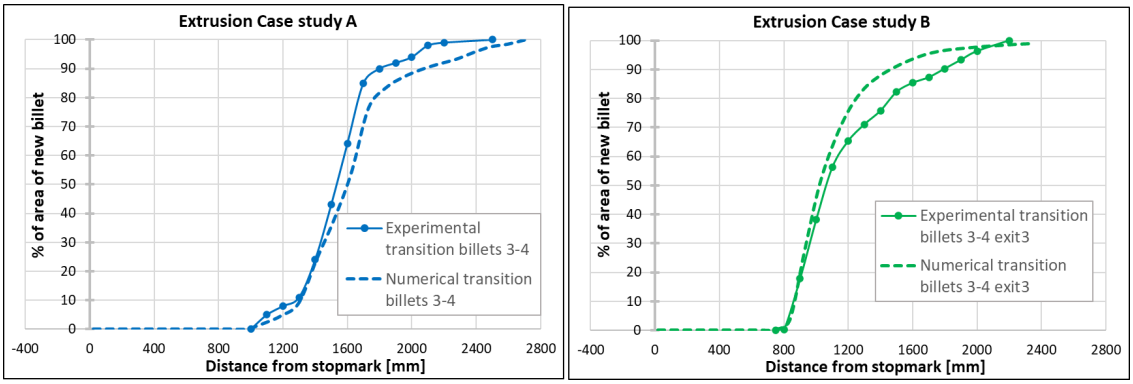

Figure 7 – Experimental-Numerical comparison of the evolution of the charge weld defect in the Extrusion Case studies A and B.

About the *Extrusion Case Study C*, the red graph in Fig. 8 indicates that the simulation predicts the defect onset at a distance of 166 mm from the stop mark, compared to the experimentally observed 130 mm, resulting in a prediction error of approximately 27.7%. Regarding the defect extent, the simulation accurately forecasts its ending around 900 mm from the stop mark, consistent with experimental findings. Fig. 10C visually demonstrates how the simulation effectively predicts the flow of the new billet material through the profile section. The defect begins to fill the central region first and subsequently propagates, starting around 300 mm, to fill the jagged appendix and the small bulge.

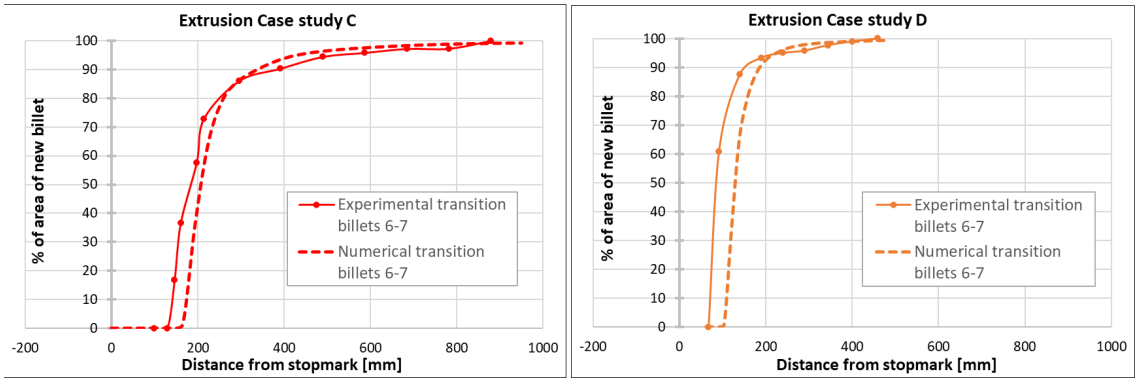

Figure 8 – Experimental-Numerical comparison of the evolution of the charge weld defect in the Extrusion Case studies C and D.

Finally for the *Extrusion Case Study D*, the numerical-experimental comparison is represented by the orange graph in Fig. 8. The simulation overestimates the defect onset, predicting it at 103 mm from the stop mark, compared to the experimentally observed 68 mm, with an error of approximately 51%. However, the simulation perfectly predicts the defect extent, matching the experimentally observed 460 mm. Similarly, Fig. 10D visually highlights that the simulation underestimates the initiation of the charge weld defect. At 92 mm from the stop mark, the new billet material is not yet apparent in the simulation. Nevertheless, despite this delay, the predicted evolution of the charge weld defect aligns with the real progression, starting from the center of the section and spreading outward.

It is worth noting that in both *Case Studies C and D*, the numerical simulation underestimated the onset of the charge weld defect, with errors of 27.7% and 51%, respectively—calculated as the percentage difference between the experimental and numerical distances relative to the actual experimental distance—which in absolute terms correspond to only 36 mm and 35 mm, when compared to the experimentally observed onset, while accurately predicts the defect extent in both cases. This discrepancy might be attributed to the skin contamination-charge interaction near the

stop-mark (Fig. 5 and Fig. 6), phenomena not simulated in the presented numerical model. Indeed, the low billet rest of 15 mm used for case studies C and D allowed the billet skin layer to enter within the die and contaminate the profile, while in the other two case studies the billet rest was enough to avoid this defect. The hypothesis is that the interaction between the new-billet material and the skin contamination has accelerated the central flow of the former, anticipating the defect's appearance. Moreover, the use of an Eulerian approach in the simulation, in which the billet is already positioned inside the die, and the filling phase, as well as the initial upsetting within the container, are not simulated, may also contribute to the numerical overestimation of the charge weld onset distance. This effect, which does not appear in case studies A and B but is evident in cases C and D, could be more pronounced for solid profiles than for hollow ones. Finally, the possibility of a simple inaccuracy of the numerical model cannot be ruled out. Therefore, further developments of this study will be focused on the prediction of skin-charge interaction.

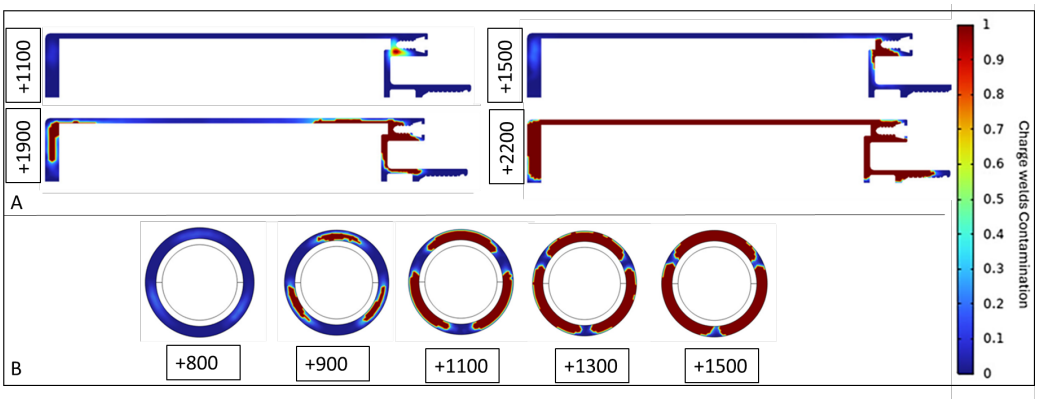

Figure 9 – Numerical analysis of the old-material replacement at different distances from the stop mark in the Extrusion Case studies A and B.

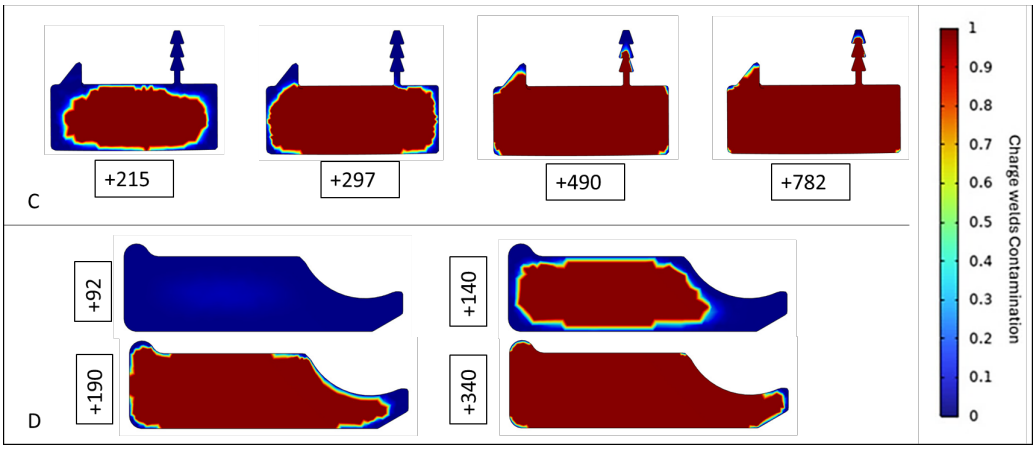

Figure 10 – Numerical analysis of the old-material replacement at different distances from the stop mark in the Extrusion Case studies C and D.

Summary

In this study, the evolution of charge weld defects during the continuous extrusion process was numerically modeled in COMSOL Multiphysics, by coupling the Navier Stokes equations with Cahn–Hilliard one for the interaction between immiscible fluids. The numerical trends demonstrated good agreement with experimental results, highlighting the predictive capability of the proposed model. Regarding Case Studies A and B the replacement of old billet material was well-predicted, with minor discrepancies in the total length of the discarded profile (errors around 8%). For Case Studies C and D, the simulation exhibited larger errors in predicting the defect onset, with deviations ranging from 25% to 50%. However, the extent of the defect, defined as the

distance at which the new billet material completely filled the profile section, was accurately predicted. It is noteworthy that the higher errors in Case Studies C and D could be attributed to the challenges of experimental measurements in these profiles, where the charge weld defect interacted with the skin defect. Further studies are required to implement skin-charge interaction as well as the presence of lubricants (multiple fluid-interaction), which can modify the defect evolution.

Fundings
PNRR–M4C2INV1.5, NextGenerationEU-Avviso 3277/2021 -ECS_00000033-ECOSISTER-spk 3

References

[1] R. Akeret, Properties of pressure welds in extruded aluminum alloy sections, J. Inst. Met 10 (1972) 202.

[2] G.J. Oberhausen, A.A.A. Christopher, D.R. Cooper, Reducing Aluminum Extrusion Transverse Weld Process Scrap, in: G. Daehn, J. Cao, B. Kinsey, E. Tekkaya, A. Vivek, Y. Yoshida (Eds.), Forming the Future, Springer International Publishing, Cham, 2021: pp. 1003–1019. https://doi.org/10.1007/978-3-030-75381-8_84

[3] Ö. Ayer, İ. Karakaya, Investigation of welding quality and internal elongation problem in aluminum extrusion, Journal of Manufacturing Processes 106 (2023) 254–264. https://doi.org/10.1016/j.jmapro.2023.10.001

[4] Y. Mahmoodkhani, M.A. Wells, N. Parson, W.J. Poole, Numerical modelling of the material flow during extrusion of aluminium alloys and transverse weld formation, Journal of Materials Processing Technology 214 (2014) 688–700. https://doi.org/10.1016/j.jmatprotec.2013.09.028

[5] Y. Mahmoodkhani, M. Wells, N. Parson, C. Jowett, W. Poole, Modeling the Formation of Transverse Weld during Billet-on-Billet Extrusion, Materials 7 (2014) 3470–3480. https://doi.org/10.3390/ma7053470

[6] J. Yu, G. Zhao, L. Chen, Investigation of interface evolution, microstructure and mechanical properties of solid-state bonding seams in hot extrusion process of aluminum alloy profiles, Journal of Materials Processing Technology 230 (2016) 153–166. https://doi.org/10.1016/j.jmatprotec.2015.11.020

[7] Z. He, H. Wang, M. Wang, G. Li, Simulation of extrusion process of complicated aluminium profile and die trial, Transactions of Nonferrous Metals Society of China 22 (2012) 1732–1737. https://doi.org/10.1016/S1003-6326(11)61380-0

[8] Q. Li, C. Harris, M.R. Jolly, Finite element modelling simulation of transverse welding phenomenon in aluminium extrusion process, Materials & Design 24 (2003) 493–496. https://doi.org/10.1016/S0261-3069(03)00123-7

[9] M. Negozio, R. Pelaccia, L. Donati, B. Reggiani, T. Pinter, L. Tomesani, Finite Element Model Prediction of Charge Weld Behaviour in AA6082 and AA6063 Extruded Profiles, J. of Materi Eng and Perform 30 (2021) 4691–4699. https://doi.org/10.1007/s11665-021-05752-x

[10] M. Negozio, R. Pelaccia, L. Donati, B. Reggiani, L. Tomesani, T. Pinter, FEM Validation of Front End and Back End Defects Evolution in AA6063 and AA6082 Aluminum Alloys Profiles, Procedia Manufacturing 47 (2020) 202–208. https://doi.org/10.1016/j.promfg.2020.04.178

[11] M. Negozio, R. Pelaccia, L. Donati, B. Reggiani, S. Di Donato, Validation of charge welds and skin contamination FEM predictions in the extrusion of a AA6082 aluminum alloy, in: 2023: pp. 86–93. https://doi.org/10.21741/9781644902714-11

[12] S. Di Donato, R. Pelaccia, M. Negozio, Phase Field Method for the Assessment of the New-Old Billet Material Interaction during Continuous Extrusion Using COMSOL Multiphysics, J.ofMateriEngandPerform(2024). https://doi.org/10.1007/s11665-024-10013-8

[13] M. Negozio, L. Donati, R. Pelaccia, B. Reggiani, S. Di Donato, Experimental analysis and modeling of the recrystallization behaviour of a AA6060 extruded profile, in: 2023: pp. 477–486. https://doi.org/10.21741/9781644902479-52

[14] R. Pelaccia, M. Negozio, S.D. Donato, L. Donati, B. Reggiani, Recent Trends in Nitrogen Cooling Modelling of Extrusion Dies, Key Engineering Materials 987 (2024) 11–22. https://doi.org/doi:10.4028/p-Q0NDkB

[15] R. Pelaccia, M. Negozio, S. Di Donato, B. Reggiani, L. Donati, Extrusion Benchmark 2023: Effect of Die Design on Profile Speed, Seam Weld Quality and Microstructure of Hollow Tubes, Key Engineering Materials 988 (2024) 47–62. https://doi.org/10.4028/p-gNXRC5

[16] R. Pelaccia, M. Negozio, S. Di Donato, B. Reggiani, L. Donati, Numerical simulation of the extrusion process with different FEM code approaches: analysis of thermal field, profile speed, defects evolution, and microstructure of hollow tubes, in: 2024: pp. 771–780. https://doi.org/10.21741/9781644903131-85

[17] M. Negozio, A. Segatori, R. Pelaccia, B. Reggiani, S. Di Donato, L. Donati, Modeling of recrystallization behaviour of AA6xxx aluminum alloy during extrusion process, Transactions of Nonferrous Metals Society of China 34 (2024) 3170–3184. https://doi.org/10.1016/S1003-6326(24)66600-8

[18] B. Reggiani, L. Donati, Prediction of liquid nitrogen die cooling effect on the extrusion process parameters by means of FE simulations and experimental validation, Journal of Manufacturing Processes 41 (2019) 231–241. https://doi.org/10.1016/j.jmapro.2019.04.002

[19] E. Giarmas, D. Tzetzis, Optimization of die design for extrusion of 6xxx series aluminum alloys through finite element analysis: a critical review, Int J Adv Manuf Technol 119 (2022) 5529–5551. https://doi.org/10.1007/s00170-022-08694-3

[20] L. Donati, B. Reggiani, R. Pelaccia, M. Negozio, S. Di Donato, Advancements in extrusion and drawing: a review of the contributes by the ESAFORM community, Int J Mater Form 15 (2022) 41. https://doi.org/10.1007/s12289-022-01664-w

[21] R. Pelaccia, P.E. Santangelo, A Homogeneous Flow Model for nitrogen cooling in the aluminum-alloy extrusion process, International Journal of Heat and Mass Transfer 195 (2022) 123–202. https://doi.org/10.1016/j.ijheatmasstransfer.2022.123202

[22] X. Zhuang, S. Zhou, G.D. Huynh, P. Areias, T. Rabczuk, Phase field modeling and computer implementation: A review, Engineering Fracture Mechanics 262 (2022) 108234. https://doi.org/10.1016/j.engfracmech.2022.108234

[23] J. Kim, Phase-Field Models for Multi-Component Fluid Flows, Commun. Comput. Phys. 12 (2012) 613–661. https://doi.org/10.4208/cicp.301110.040811a

[24] R. Pelaccia, B. Reggiani, M. Negozio, L. Donati, Liquid nitrogen in the industrial practice of hot aluminium extrusion: experimental and numerical investigation, Int J Adv Manuf Technol 119 (2022) 3141–3155. https://doi.org/10.1007/s00170-021-08422-3